Structural changes in mixed Col I/Col V collagen gels probed by SHG microscopy: implications for probing stromal alterations in human breast cancer

Visar Ajeti,[1,2] Oleg Nadiarnykh,[3] Suzanne M. Ponik,[2,4] Patricia J. Keely,[1,2,4] Kevin W. Eliceiri,[1,2] and Paul J. Campagnola[1,2,*]

[1]*Department of Biomedical Engineering, University of Wisconsin-Madison, Madison, Wisconsin 53706, USA*
[2]*Laboratory for Optical and Computational Instrumentation (LOCI), University of Wisconsin-Madison, Madison Wisconsin 53706, USA*
[3]*Present Address: Department of Physics, University of Utrecht, The Netherlands*
[4]*Department of Cell and Regenerative Biology, University of Wisconsin-Madison, Madison, Wisconsin 53706, USA*
**pcampagnola@wisc.edu*

Abstract: Second Harmonic Generation (SHG) microscopy has been previously used to describe the morphology of collagen in the extracellular matrix (ECM) in different stages of invasion in breast cancer. Here this concept is extended by using SHG to provide quantitative discrimination of self-assembled collagen gels, consisting of mixtures of type I (Col I) and type V (Col V) isoforms which serve as models of changes in the ECM during invasion in vivo. To investigate if SHG is sensitive to changes due to Col V incorporation into Col I fibrils, gels were prepared with 0-20% Col V with the balance consisting of Col I. Using the metrics of SHG intensity, fiber length, emission directionality, and depth-dependent intensities, we found similar responses for gels comprised of 100% Col I, and 95% Col I/5% Col V, where these metrics were all significantly different from those of the 80% Col I/20% Col V gels. Specifically, the gels of lower Col V content produce brighter SHG, are characterized by longer fibers, and have a higher forward/backward emission ratio. These attributes are all consistent with more highly organized collagen fibrils/fibers and are in agreement with previous TEM characterization as well as predictions based on phase matching considerations. These results suggest that SHG can be developed to discriminate Col I/Col V composition in tissues to characterize and follow breast cancer invasion.

OCIS codes: (180.6900) Three-dimensional microscopy; (190.4180) Multiphoton processes; (190.2620) Harmonic generation and mixing; (290.7050) Turbid media; (170.6935) Tissue characterization.

References and links

1. C. Ricciardelli and R. J. Rodgers, "Extracellular matrix of ovarian tumors," Semin. Reprod. Med. **24**(4), 270–282 (2006).
2. S. M. Pupa, S. Ménard, S. Forti, and E. Tagliabue, "New insights into the role of extracellular matrix during tumor onset and progression," J. Cell. Physiol. **192**(3), 259–267 (2002).
3. N. Théret, O. Musso, B. Turlin, D. Lotrian, P. Bioulac-Sage, J. P. Campion, K. Boudjéma, and B. Clément, "Increased extracellular matrix remodeling is associated with tumor progression in human hepatocellular carcinomas," Hepatology **34**(1), 82–88 (2001).
4. P. M. McGowan and M. J. Duffy, "Matrix metalloproteinase expression and outcome in patients with breast cancer: analysis of a published database," Ann. Oncol. **19**(9), 1566–1572 (2008).
5. J. M. Pellikainen, K. M. Ropponen, V. V. Kataja, J. K. Kellokoski, M. J. Eskelinen, and V. M. Kosma, "Expression of matrix metalloproteinase (MMP)-2 and MMP-9 in breast cancer with a special reference to activator protein-2, HER2, and prognosis," Clin. Cancer Res. **10**(22), 7621–7628 (2004).

#148528 - $15.00 USD Received 31 May 2011; revised 12 Jul 2011; accepted 14 Jul 2011; published 20 Jul 2011

6. S. Y. Huang, M. Van Arsdall, S. Tedjarati, M. McCarty, W. J. Wu, R. Langley, and I. J. Fidler, "Contributions of stromal metalloproteinase-9 to angiogenesis and growth of human ovarian carcinoma in mice," J. Natl. Cancer Inst. **94**(15), 1134–1142 (2002).
7. H. Hugo, M. L. Ackland, T. Blick, M. G. Lawrence, J. A. Clements, E. D. Williams, and E. W. Thompson, "Epithelial--mesenchymal and mesenchymal--epithelial transitions in carcinoma progression," J. Cell. Physiol. **213**(2), 374–383 (2007).
8. T. Sørlie, C. M. Perou, R. Tibshirani, T. Aas, S. Geisler, H. Johnsen, T. Hastie, M. B. Eisen, M. van de Rijn, S. S. Jeffrey, T. Thorsen, H. Quist, J. C. Matese, P. O. Brown, D. Botstein, P. Eystein Lønning, and A. L. Børresen-Dale, "Gene expression patterns of breast carcinomas distinguish tumor subclasses with clinical implications," Proc. Natl. Acad. Sci. U.S.A. **98**(19), 10869–10874 (2001).
9. P. J. Campagnola and L. M. Loew, "Second-harmonic imaging microscopy for visualizing biomolecular arrays in cells, tissues and organisms," Nat. Biotechnol. **21**(11), 1356–1360 (2003).
10. Y. R. Shen, *The Principles of Nonlinear Optics* (John Wiley and Sons, 1984).
11. S. V. Plotnikov, A. C. Millard, P. J. Campagnola, and W. A. Mohler, "Characterization of the myosin-based source for second-harmonic generation from muscle sarcomeres," Biophys. J. **90**(2), 693–703 (2006).
12. R. Lacomb, O. Nadiarnykh, S. S. Townsend, and P. J. Campagnola, "Phase Matching considerations in Second Harmonic Generation from tissues: Effects on emission directionality, conversion efficiency and observed morphology," Opt. Commun. **281**(7), 1823–1832 (2008).
13. R. M. Williams, W. R. Zipfel, and W. W. Webb, "Interpreting second-harmonic generation images of collagen I fibrils," Biophys. J. **88**(2), 1377–1386 (2005).
14. F. Légaré, C. Pfeffer, and B. R. Olsen, "The role of backscattering in SHG tissue imaging," Biophys. J. **93**(4), 1312–1320 (2007).
15. P. P. Provenzano, K. W. Eliceiri, J. M. Campbell, D. R. Inman, J. G. White, and P. J. Keely, "Collagen reorganization at the tumor-stromal interface facilitates local invasion," BMC Med. **4**(1), 38 (2006).
16. P. P. Provenzano, D. R. Inman, K. W. Eliceiri, J. G. Knittel, L. Yan, C. T. Rueden, J. G. White, and P. J. Keely, "Collagen density promotes mammary tumor initiation and progression," BMC Med. **6**(1), 11 (2008).
17. M. W. Conklin, J. C. Eickhoff, K. M. Riching, C. A. Pehlke, K. W. Eliceiri, P. P. Provenzano, A. Friedl, and P. J. Keely, "Aligned collagen is a prognostic signature for survival in human breast carcinoma," Am. J. Pathol. **178**(3), 1221–1232 (2011).
18. E. Sahai, J. Wyckoff, U. Philippar, J. E. Segall, F. Gertler, and J. Condeelis, "Simultaneous imaging of GFP, CFP and collagen in tumors in vivo using multiphoton microscopy," BMC Biotechnol. **5**(1), 14 (2005).
19. S. J. Lin, S. H. Jee, C. J. Kuo, R. J. Wu, W. C. Lin, J. S. Chen, Y. H. Liao, C. J. Hsu, T. F. Tsai, Y. F. Chen, and C. Y. Dong, "Discrimination of basal cell carcinoma from normal dermal stroma by quantitative multiphoton imaging," Opt. Lett. **31**(18), 2756–2758 (2006).
20. R. Cicchi, S. Sestini, V. De Giorgi, P. Carli, D. Massi, and F. S. Pavone, "Basal cell carcinoma imaging and characterization by multiple nonlinear microscopy techniques," Biophys. J., 157a–157a (2007).
21. E. Brown, T. McKee, E. diTomaso, A. Pluen, B. Seed, Y. Boucher, and R. K. Jain, "Dynamic imaging of collagen and its modulation in tumors in vivo using second-harmonic generation," Nat. Med. **9**(6), 796–801 (2003).
22. O. Nadiarnykh, R. B. LaComb, M. A. Brewer, and P. J. Campagnola, "Alterations of the extracellular matrix in ovarian cancer studied by Second Harmonic Generation imaging microscopy," BMC Cancer **10**(1), 94 (2010).
23. S. H. Barsky, C. N. Rao, G. R. Grotendorst, and L. A. Liotta, "Increased content of Type V Collagen in desmoplasia of human breast carcinoma," Am. J. Pathol. **108**(3), 276–283 (1982).
24. D. E. Birk, J. M. Fitch, J. P. Babiarz, K. J. Doane, and T. F. Linsenmayer, "Collagen fibrillogenesis in vitro: interaction of types I and V collagen regulates fibril diameter," J. Cell Sci. **95**(Pt 4), 649–657 (1990).
25. P. J. Keely, A. M. Fong, M. M. Zutter, and S. A. Santoro, "Alteration of collagen-dependent adhesion, motility, and morphogenesis by the expression of antisense alpha 2 integrin mRNA in mammary cells," J. Cell Sci. **108**(Pt 2), 595–607 (1995).
26. O. Nadiarnykh, R. B. Lacomb, P. J. Campagnola, and W. A. Mohler, "Coherent and incoherent SHG in fibrillar cellulose matrices," Opt. Express **15**(6), 3348–3360 (2007).
27. D. J. Hulmes, "Building collagen molecules, fibrils, and suprafibrillar structures," J. Struct. Biol. **137**(1-2), 2–10 (2002).
28. B. Eyden and M. Tzaphlidou, "Structural variations of collagen in normal and pathological tissues: role of electron microscopy," Micron **32**(3), 287–300 (2001).
29. D. E. Birk, "Type V collagen: heterotypic type I/V collagen interactions in the regulation of fibril assembly," Micron **32**(3), 223–237 (2001).
30. R. Lacomb, O. Nadiarnykh, and P. Campagnola, "Quantitative second harmonic generation imaging of the diseased state osteogenesis imperfecta: experiment and simulation," Biophys. J. **94**(11), 4504–4514 (2008).
31. R. LaComb, O. Nadiarnykh, S. Carey, and P. J. Campagnola, "Quantitative second harmonic generation imaging and modeling of the optical clearing mechanism in striated muscle and tendon," J. Biomed. Opt. **13**(2), 021109 (2008).
32. C. B. Raub, V. Suresh, T. Krasieva, J. Lyubovitsky, J. D. Mih, A. J. Putnam, B. J. Tromberg, and S. C. George, "Noninvasive assessment of collagen gel microstructure and mechanics using multiphoton microscopy," Biophys. J. **92**(6), 2212–2222 (2007).

#148528 - $15.00 USD Received 31 May 2011; revised 12 Jul 2011; accepted 14 Jul 2011; published 20 Jul 2011

33. F. Tiaho, G. Recher, and D. Rouède, "Estimation of helical angles of myosin and collagen by second harmonic generation imaging microscopy," Opt. Express **15**(19), 12286–12295 (2007).
34. P. J. Su, W. L. Chen, Y. F. Chen, and C. Y. Dong, "Determination of collagen nanostructure from second-order susceptibility tensor analysis," Biophys. J. **100**(8), 2053–2062 (2011).
35. C. Luparello, F. David, G. Campisi, and R. Sirchia, "T47-D cells and type V collagen: a model for the study of apoptotic gene expression by breast cancer cells," Biol. Chem. **384**(6), 965–975 (2003).
36. X. X. Han and E. Brown, "Measurement of the ratio of forward-propagating to back-propagating second harmonic signal using a single objective," Opt. Express **18**(10), 10538–10550 (2010).

1. Introduction

For women in the US, death rates from breast cancer are the second highest among all cancers, and approximately 1 in 8 will develop the disease during their lifetime. Thus there remains a compelling need for new technologies that have both sufficient resolution and specificity to detect microscopic tumors or precursor lesions. Probing for alterations in the extracellular matrix (ECM) composition and structure may be a promising approach in this regard, as these changes are thought to be critical for tumor initiation and progression for several epithelial carcinomas [1–3]. For example, up-regulation of several proteases (e.g. MMP-1, MMP-9, and MMP-14) in breast cancer has been implicated in invasion/metastasis where these act by degrading the basement membrane and/or stroma [4,5]. Additionally, in a feed-forward mechanism, changes in the stromal compartment of a tumor can then elicit a cascade of further changes involving fibroblasts and tumor cells thereby generating more aggressive tumor cells [6,7]. Moreover, certain subtypes of breast cancer are thought to carry the necessary gene expression characteristics that promote very early metastasis at the time that they become invasive [8], such that routine screening modalities will fail to detect them early enough to impact survival. We propose that changes in the ECM may be a biomarker of invasion and these will provide insight into the factors that facilitate this process.

To investigate this possibility, we have explored the use of high resolution Second Harmonic Generation (SHG) imaging microscopy [9] to quantify differences in tissue structure using in vitro fibrillar models of the ECM for breast cancer. SHG is a coherent nonlinear process wherein two lower energy photons are up-converted to exactly twice the incident frequency (or half the wavelength) of an excitation laser [10]. Due to the second order symmetry constraints imposed by the underlying physics, the SHG contrast vanishes for assemblies with mirror symmetry (i.e. centro-symmetric environment) and increases for well-ordered structures [9]. Thus the relative alignment of fibrils/fibers is reflected in the magnitude of $\chi^{(2)}$ which is experimentally manifested in the SHG intensity. This tensor further contains information on the alignment of the collagen molecules in the fibrils/fibers [11]. Additionally, SHG has a well-defined emission direction (i.e. the forward-backward ratio) that carries information related to the sub-resolution size and packing of the fibrils and fibers [12–14].

SHG has already been shown to have potential applicability for cancer diagnosis by revealing changes in the ECM in tumors (breast and other epithelial cancers) relative to normal tissues. Using mouse as well as in vitro models of breast carcinoma, Keely [15,16] identified distinct stages of invasion by measuring changes of the angle of collagen fibers with respect to tumor boundaries. They also utilized SHG to measure collagen orientation in human breast cancer histopathology slides and showed that quantifying the alignment could be used as a predictive tool for patient survival rate [17]. Condeelis further showed how invasive cancer cells used collagen fibers to facilitate migration in vivo [18]. The Dong [19] and Pavone [20] labs used SHG to identify tumor borders in basal cell carcinoma lesions by imaging the collagen assembly. Jain et al took a similar approach in imaging melanoma in a mouse model [21]. Campagnola and associates used SHG to visualize striking morphological changes in malignant human ovarian biopsies and further showed how several SHG signatures were correlated with sub-resolution structural changes, which collectively indicated that the diseased tissues were more highly organized than the corresponding normal [22].

#148528 - $15.00 USD Received 31 May 2011; revised 12 Jul 2011; accepted 14 Jul 2011; published 20 Jul 2011

In sum, these previous studies have demonstrated clear and quantifiable changes in the overall fibrillar collagen content that occur in several epithelial cancers. A parallel issue that has not been explored is if the effects of changes in the distribution of collagen isoforms on ECM structure can be probed by SHG microscopy. For example, up-regulation of Col V has been implicated in human breast cancer. This is a minor isoform that is normally present in connective tissues (~1% total collagen) but not found within normal breast stroma, which is primarily Col I. However, Liotta showed in 1982 that this isoform can constitute up to 20% of the total collagen content in the stroma in carcinomas [23]. Birk et al later made self-assembled fibrillar gels of varying Col V fractions and through transmission electron microscopy (TEM) measurements showed that increased Col V concentration resulted in thinner, less organized fibrils that lacked the typical periodicity seen in type I collagen [24]. Here we continue this work by synthesizing analogous fibrillar Col I/Col V collagen gels and use SHG to quantify changes in the collagen assembly due to changes in the isoform distribution. SHG has the advantage over TEM in being able to image noninvasively through intact 3D tissues with relatively large fields of view. While SHG lacks the resolution of EM, it provides structural information at both the fibril and fiber levels of organization due to the coherence of the process [12], and we will show how the SHG metrics of intensity, and emission directionality, (forward to backward ratio) are consistent with ultra-structural findings.

2. Methods

2.1 Col I/Col V Collagen Gels

The collagen gels were polymerized as previously described [25]. Briefly, type I rat-tail collagen (BD Biosciences) and type V human placental collagen (Sigma Aldrich) were neutralized with an equal volume of 100 mM HEPES in 2X PBS to obtain 1 mg/ml collagen gels comprised of a mixture of Type I/ Type V collagen at fractions of 100/0, 99/1, 95/5, or 80/20%. A total gel volume of 1 ml was achieved by the addition of serum-free RPMI media (Gibco). The collagen gel solution was polymerized in a 6-well tissue culture dish overnight at 37°C, then the gels were released from the bottoms and sides of the dish, and fixed in 4% paraformaldehyde. Each series of comparisons of the SHG signatures from the different compositions were carried out with gels polymerized at the same time and the results for each concentration are thus internally self-consistent.

2.2 Western Blots

Protein expression was assessed through immunoblotting. Briefly, gels were lysed in denaturing Laemmli buffer followed by protein separation using SDS-PAGE. After proteins were transferred onto PVDF membrane, membranes were blocked using 5% milk plus 0.3% Tween-20 in TBS. Membranes were probed with 1:1000 anti-Col V (Abcam**)** followed by incubation with 1:5000 HRP-conjugated secondary antibody. Membranes were visualized using pico-ECL reagent (Amersham Biosciences) and exposed to x-ray film.

2.3 SHG Microscope

The utilized SHG imaging system has been described in detail elsewhere and is only briefly described here [11]. The instrument consists of a laser scanning unit (Fluoview 300; Olympus) mounted on an upright microscope stand (BX61, Olympus), coupled to a mode-locked Titanium Sapphire femtosecond laser (Mira; Coherent). All SHG imaging was performed with an excitation wavelength of 890 nm with an average power of ~20 mW at the specimen using a water immersion 40x 0.8 NA objective, and the forward SHG was collected with a 0.9 NA condenser. This wavelength and NA resulted in lateral and axial resolutions (FWHM) of approximately 0.7 and 2.5 microns, respectively. SHG images were obtained using circularly polarized excitation as this probes all fiber orientations equally. The desired

#148528 - $15.00 USD Received 31 May 2011; revised 12 Jul 2011; accepted 14 Jul 2011; published 20 Jul 2011

polarization at the focus was achieved as previously described [26]. The microscope simultaneously collects both the forward (F) and backward (B) components of the SHG intensity using identical, calibrated detectors (7421 GaAsP photon counting modules; Hamamatsu) and the remainder of the optical paths [26]. The SHG wavelength (445 nm for 890 excitation wavelength) was isolated with a 20 nm wide 445 bandpass filter (Semrock). 3D renderings were performed with Imaris visualization software (Bitplane).

2.4 3D SHG Imaging Measurements

The measured depth dependence of the forward-backward intensity ratio (F/B) of the SHG signal is one means to characterize structural changes in collagen organization. The measured SHG directional (F/B ratios) values were determined by integration of the intensity of 5-10 frames per optical section every two microns of depth using ImageJ software (http://rsb.info.nih.gov/ij/). The measured attenuation, i.e. rate of intensity decrease with increasing depth into tissue, of the forward SHG signal is also used to characterize structural changes in the ECM. To this end the data of each optical series for each gel is self-normalized to the optical section with the average maximum intensity. The normalized forward attenuation data was taken concurrently with the F/B data. Like the directional data, these measurements are quantitated using ImageJ by integration over whole fields of view. Fiber lengths were measured in ImageJ, where the images were thresholded and then fiber lengths were measured manually using the drawing tool.

3. Results

3.1 Gel Characterization

We sought to create Col I/Col V mixed gels that reflect the collagen V content representative in normal breast stroma (0% col V) and the stroma during invasive carcinoma (95%/5% and 80%/20% Col I and Col V, respectively). Figure 1 shows the resulting Western blots used to verify the overall incorporation of the two components. An attempt was made to create gels of 99%/1% composition but these were indistinguishable by Western blots from the 100% Col I. While the intensity of the 100% Col I in the blots was saturated, these showed that the intensity of the loaded 20% was ~2.4 greater than that of the 5%. This could be either reflective of the actual incorporation or the only semi-quantitative nature of the analysis. Here we use it as a guideline through which to assess the SHG data.

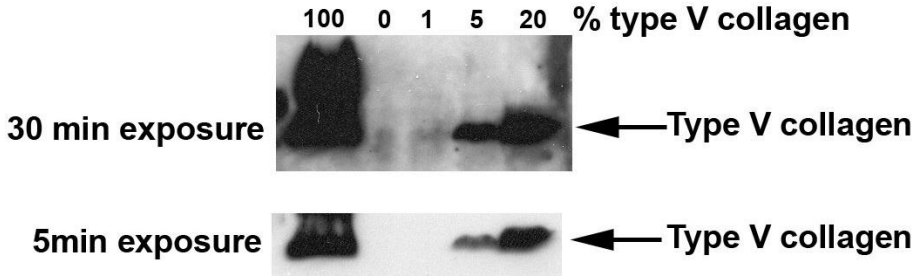

Fig. 1. Western blots of the collagen gels showing the Col V incorporation.

Figure 2 shows the resulting 3D renderings (using the shadowing feature) from SHG z dimensional stacks of each of these gels, where the intensities are scaled for presentation. The 100% Col I and 95%/5% Col I/Col V gels have similar structure and intensity (raw data). The 80/20 Col I/Col V gels are characterized by shorter, more closely packed fibers. The raw intensity of this gel (integrated over the whole volume) was 3-fold less than the gels of greater Col I concentration, indicating decreased organization due to the higher Col V concentration.

#148528 - $15.00 USD Received 31 May 2011; revised 12 Jul 2011; accepted 14 Jul 2011; published 20 Jul 2011

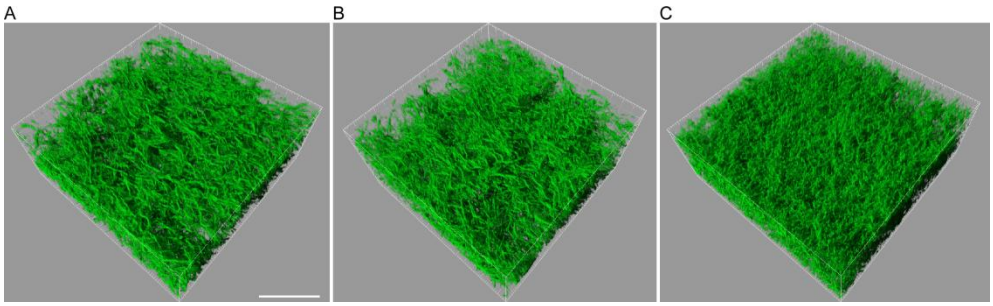

Fig. 2. 3D SHG renderings of (A) 100% Col I, (b) 95% Col I/5% Col V, and (c) 80% Col I/20% Col V collagen gels. Scale bar = 50 microns.

To further explore the result of Col V incorporation into the collagen fibers, representative single optical sections for the gels are shown in Fig. 3. Figure 3(c) and Fig. 3(d) are the respective raw and scaled (by the average intensity) images of the 80% Col I /20% Col V gel. We determined the fiber lengths (Fig. 3(e)) for the three compositions of 0, 5, and 20% Col V collagen, where this yielded average values of 23.2 ± 2.4, 20.5 ± 1.8, and 12.4 ± 1.7 microns, respectively, where the error bars represent standard deviations. For each composition, the average fiber length was significantly different than the others ($p<0.001$) by paired-sample t-tests.

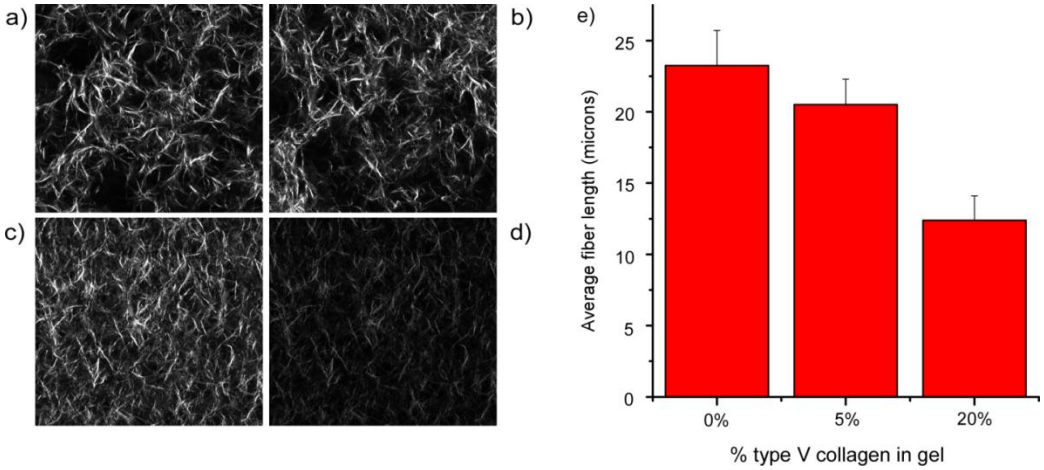

Fig. 3. Single optical sections of the (a) 100% Col I, (b) 95% Col I/5% Col /V and (c and d) 80% Col I /20% Col V collagen gels, where (d) shows the raw intensity at the same laser intensity as for the gels in (a) and (b). Field size = 170 microns. (e) Average fiber lengths, where the error bars represent standard deviations.

As fibers are formed by additional crosslinking of fibrils [27], it is physically consistent that the fibers would be smaller as well. As an example, in the connective tissue disorder osteogenesis imperfecta (OI) smaller, more disorganized fibrils result in the assembly into smaller fibers [28]. For the collagen mixtures discussed here Birk et al previously reported average fibril diameters of approximately 150 nm for compositions between 0 and 10% Col V, about 100 nm for the 80/20% gel, and 25 nm for gels of 100% Col V [24]. They presented a model of assembly for Col I/Col V fibrils, where latter component is buried within the core, but the terminal amine lies fibril perpendicular to the long axis [24]. The helical region extends through the hole-zone to the surface and acts as a flexible hinge, hindering additional crosslinking, and thereby limits the size of the fibril [29].

#148528 - $15.00 USD Received 31 May 2011; revised 12 Jul 2011; accepted 14 Jul 2011; published 20 Jul 2011

3.2 SHG Directionality (F/B) and Fibril Organization in Mixed Col I/ Col V Collagen Gels

We have previously used the measured depth dependence of the SHG forward-backward ratio (F/B) as a means to compare the fibril size and assembly in tissue structures. For example, we used this metric in analytic comparison between normal and diseased states (e.g. ovarian cancer, and osteogenesis imperfecta) [22,30] as well as interpreting the mechanism of optical clearing [31]. This axial response arises from a convolution between the initial SHG directional emission ratio (which we denote F_{SHG}/B_{SHG}) and subsequent SHG propagation through the tissue, which is based on the bulk optical parameters μ_s (scattering coefficient) and g (scattering anisotropy) at λ_{SHG}. The F_{SHG}/B_{SHG} is highly dependent upon the fibril diameter, the packing density, and also the regularity relative to the size-scale of the SHG wavelength [12]. For example, as the dimensions of fibrils, or assembly thereof, in the axial direction approach λ_{SHG}, the emitted SHG becomes increasingly forward directed, whereas for small fibrils (e.g. $\lambda_{SHG}/10$) this ratio approaches unity [12]. In tissues in general, Monte Carlo simulations are required to decouple F_{SHG}/B_{SHG} from the resulting propagation as the source of the measured photons are experimentally indistinguishable. However, the fibrillar gels employed here are not sufficiently dense to induce multiple scattering events (~1 scattering length), the measured F/B is similar to the emitted distribution. The gels have approximately the same thickness, and were prepared with the same total protein concentration, and thus should be affected by scattering to a similar extent.

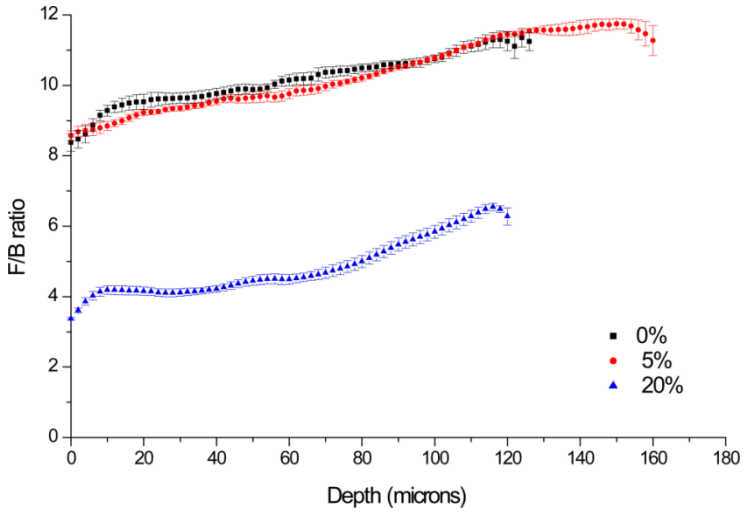

Fig. 4. Measured SHG F/B vs depth for the gels shown in Fig. 2 and 3.

The resulting axially dependent F/B data from a set of gels prepared simultaneously (same set as shown in Figs. 2 and 3) is shown in Fig. 4. We found highly forward directed SHG for all cases, where the 0, and 5% Col V gels are indistinguishable and the F/B increases from ~8-11 over the range of 100 microns of thickness. The 80%/20% gel displays a lower value of ~4-6 over this same range. Based on using similar fibril diameter distribution for the 0% and 5% Col V gels [24], in our model of SHG phasematching [12], we predicted a similar F/B response. This is because, in the absence of multiple scattering, this metric reflects the F_{SHG}/B_{SHG} emitted distribution, which as we have previously shown arises from the fibril size and alignment in the axial direction with respect to the laser propagation. In contrast, the 20% Col V gel has a smaller measured F/B, which would be expected for a structure comprised of smaller, more randomly distributed fibrils.

We stress that the emission directionality F_{SHG}/B_{SHG} depends on the phase mismatch Δk, which arises from a combination of the fibril size and packing and is not directly measurable. Moreover, the mismatch is likely represented by a distribution of Δk values rather than being

#148528 - $15.00 USD Received 31 May 2011; revised 12 Jul 2011; accepted 14 Jul 2011; published 20 Jul 2011

single valued due to the inherent randomness in biological tissues. Still, through this analysis we showed that smaller, more random assemblies of fibrils would be associated with B_{SHG} (and lower F/B values), larger Δk values, and correspondingly weaker SHG. These predictions are consistent with the results for the 20% Col V gel relative to the 0% and 5% mixtures. Additionally, FFT analysis (not shown) found that the 20% type gel is characterized by a broader distribution of higher spatial frequencies, i.e. smaller features, where the distribution is more slowly decaying than that of the 5% type V gel, which primarily consists of primarily lower frequency components.

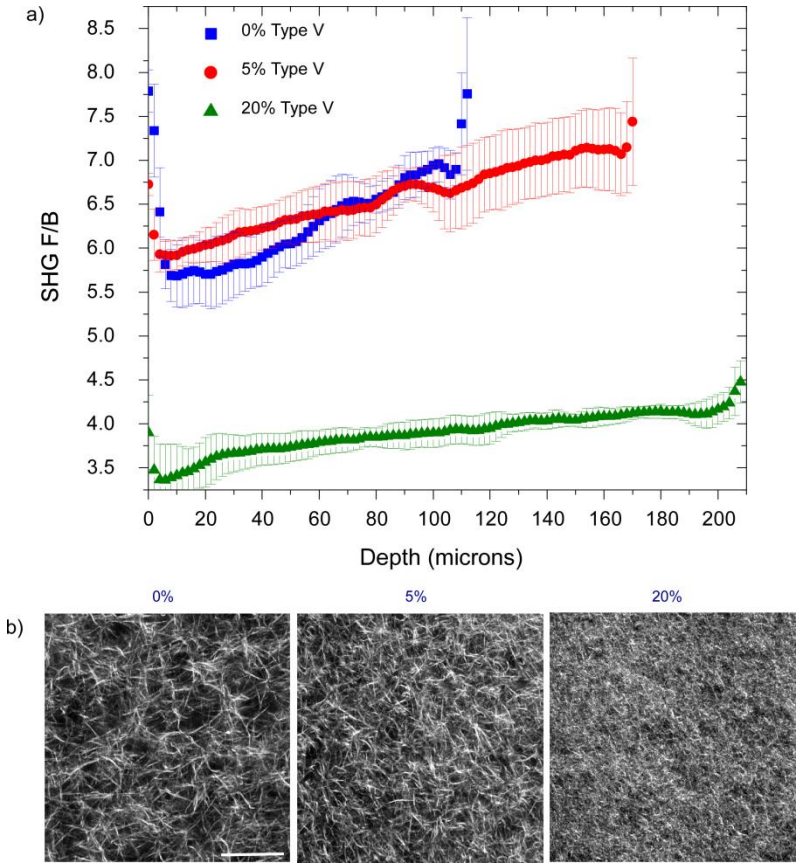

Fig. 5. **(**a) F/B data for an independent polymerization run of 0%, 5%, and 20% Col V collagen gels, where representative individual optical sections are given in the bottom panel in 5(b). Scale bar = 50 microns.

We note that the absolute F/B values depend on the preparation, as the achieved degree of collagen polymerization (and thus fibril/fiber size distribution) can vary between syntheses. It has been well-documented that the fibrillar size and density are highly sensitive to factors including the precise time and temperature both before and during polymerization [32]. However, for each set of measurements the gels of differing Col V concentration were polymerized together in the same multiwell plate and can be compared self-consistently. For example, Fig. 5a shows the axially dependent F/B measurement for an independent polymerization run, where the F/B values were somewhat lower than the data in Fig. 4, where both the 0 and 5% Col V gels had indistinguishable profiles of 5.5-6.5 over the range of 100 microns, and the data for the 20% ranged from 3.5 to 4.5 over the same thickness. Thus, while the absolute values varied, the trends were the same and self-consistent. Individual optical sections for these gels are given in Fig. 5b. Based on the respective observed fibrillar

#148528 - $15.00 USD Received 31 May 2011; revised 12 Jul 2011; accepted 14 Jul 2011; published 20 Jul 2011

morphologies, the measured F/B values are consistent in each case per the mathematical model we previously presented and discussed above [12]. Specifically the gels with the higher F/B have longer, more organized fibers ((0 and 5% Col V collagen), where the more disorganized 20% col V gel is predicted to have a lower F/B.

3.3. Axial Dependence of the Forward Directed SHG Intensity

We have previously used the measured attenuation (or rate of decay with depth) of the forward SHG intensity as a means to compare tissues [30]. This axial response results from a compounded mechanism of SHG creation attributes (the F_{SHG}/B_{SHG} emission directionality and relative SHG intensity based on $\chi^{(2)}$) and primary filter effect (loss of laser intensity due to scattering) and secondary filter effect (loss of SHG signal). Since biological tissues have intrinsic heterogeneity in concentration, we have found a normalized approach necessary to account for local variability in SHG intensities in the same tissue (different fields) and to make relative comparisons between tissues. The resulting data for the three gels (same set as in Figs. 2-4) of differing Col V concentration are shown in Fig. 6, where they are scaled relative to the maximum relative intensity at the same laser excitation power. The rapid decay at the end of the data corresponds to the exit of the tissue. In analogy to the F/B data in Figs. 4 and 5 the 0% and 5% Col V gels have similar responses, both in terms of relative intensity and intensity with increasing depth into the gel. In contrast, the 80/20% gel is about 4-fold lower in intensity.

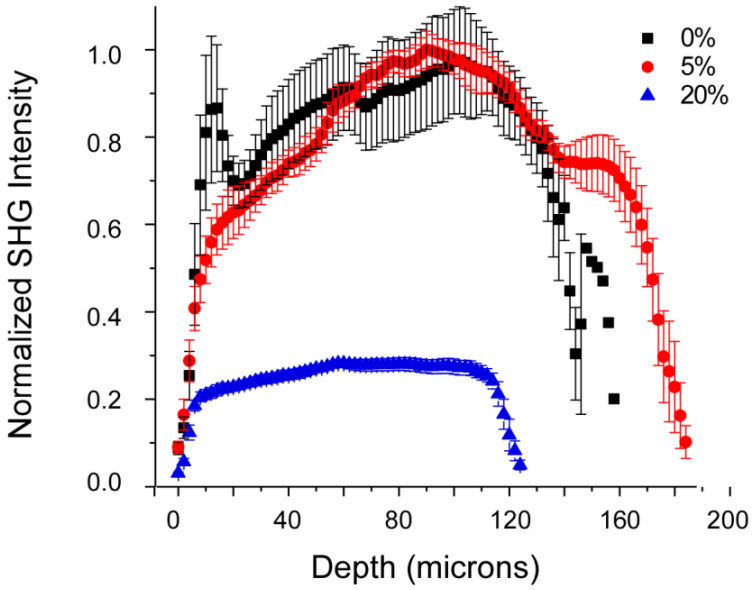

Fig. 6. Axial dependence of the forward SHG intensity for the mixed Col I/Col V gels. Similar to the directional data, the 0 and 5% Col V gels are indistinguishable, and are different from the 20% Col V gel.

We have previously described how this depth dependent measurement is highly sensitive to the relative $\chi^{(2)}$ values. Specifically, we showed how the SHG intensity built up with increasing domain size such that larger fibrils or closed packed smaller fibrils yield larger signal relative to smaller, and larger spaced fibrils. Thus based on the similar fibril/fiber structure for the gels of lower Col V content (0% and 5%), we predicted comparable second order responses. This treatment further predicts lower SHG intensity for the distribution of fibril size and packing in the 80/20% gels. Lastly, we note that the shape of the attenuation curves also depends on the relative roles of the primary and secondary filter effects

#148528 - $15.00 USD Received 31 May 2011; revised 12 Jul 2011; accepted 14 Jul 2011; published 20 Jul 2011

[22,30,31]. In these efforts we showed theoretical predictions of the attenuation and F/B over a range of scattering properties as well as using values from real tissues. In all cases we showed that the primary filter (squared) dominated the observed SHG attenuation, where the secondary filter contributes little. Based on these findings we can conclude the weak dependence of intensity on depth is indicative of weak scattering at both the laser and SHG wavelengths.

4. Discussion and Conclusions

We have shown how SHG microscopy can differentiate collagen gels of varying Col I/Col V composition through simple metrics of relative intensities, which are based on the respective $\chi^{(2)}$ values, and measurement of fiber lengths. Additionally, forward-backward SHG and attenuation measurements reflect changes in the fibril size and packing between the different sizes. Our inferences on these sub-resolution changes (~100 nm fibril diameters) are consistent with TEM measurements, which show that higher concentrations of type V collagen lead to smaller fibrils that are packed in a more disordered fashion. These smaller fibrils then organize into shorter fibers which are directly revealed in the SHG image.

We note that we also tried methods based on polarization to provide discrimination between the different compositions. We previously showed that the angular dependence of the SHG intensity is related to the helical pitch angle [11], and other reports used this approach to delineate different, spatially separated proteins in tissues [33,34]. However, in these measurements we were not able to discern any differences in the dependence of the laser excitation polarization on the SHG intensity between the different gels. Similarly, the SHG signal anisotropy, which is most sensitive to dipole alignment, did not reveal any differences.

The first evidence of up-regulation of type V collagen in the desmoplastic stroma surrounding breast carcinoma was suggested by Liotta in 1982 [23]. It was suggested that this isoform was secreted by myofibroblasts recruited in response to invasion. More recent work has shown that, in tissue culture, Col V is anti-adhesive in 8701-BC and T47-D human breast carcinoma cells, and that the cells that do adhere are induced into apoptosis through up-regulation of caspases [35]. Thus it appears that the up-regulation of this collagen isoform may represent a defense mechanism that could serve to inhibit neoplasm growth. While these 2D studies have provided insight into the progression of human breast carcinoma, more can be gained through 3D imaging studies of the ECM changes, and SHG is ideally suited to monitor these alterations. For example, future studies will perform these measurements in mixed gels seeded with human breast carcinoma cells.

Having established the sensitivity in vitro, we suggest these methods could ultimately be employed for in vivo studies. The SHG approach would first need to first be validated by immunostaining of slices. Measuring the directionality in vivo is a challenging task, however Brown recently showed how the F/B could be extracted using a single objective [36]. Still, through using our current methods, ex vivo SHG analysis in the operating room has potential for discriminating normal vs malignant tissues as the equipment continues to be reduced in size.

Acknowledgments

PJC gratefully acknowledges support under NIH EB1842; PJC, KWE, and PJK gratefully acknowledge under NIH CA136590.

#148528 - $15.00 USD Received 31 May 2011; revised 12 Jul 2011; accepted 14 Jul 2011; published 20 Jul 2011